RESULTS AND DISCUSSION

The titration data were collected by measuring the potential (E) in mV using a pH meter standardized with an acid-base titration performed daily. From the potential, the pH was determined from the equation:

$$\text{pH} = -\log[(\text{vol. acid} \times \text{conc. acid/tot. vol.}) - (\text{vol. base} \times \text{conc. base/tot. vol.})] \quad (1)$$

Once the pH was determined, a graph of E vs. pH can be shown to give a slope comparable to the Nernstian slope, 59.16 mV, where the number of protons and electrons in a redox process are equal. A plot of E vs. pH can be seen in Figure 6 for an acid-base titration. Using the slope along with the previous data, the standard electrode potential, E^o, can be calculated using

$$\frac{E^o - E}{slope} = pH \quad (2)$$

$$E^o = pH(slope) + E \quad (3)$$

The value for E^o determined for the particular cell plus glass electrode plus reference electrode used in this study ranged from 412 to 423 mV, accompanied by a deviation of the Nernstian slope from the accepted 59.16 mV. It is normal for the E^o and Nernstian slope to change for a given glass electrode, which is thought to be caused by changes in the surface structure of the glass with time. This deviation is the reason that daily calibrations of the pH meter were necessary. Determined values of the Nernstian slope obtained here ranged from 57.7 to 59.9 mV/decade.

Using this primary information, a series of mass balance equations were solved in order to obtain information on the various species of ligand found in solution. We have broken down the three species of ligand possible as bound ligand (ML), free ligand (L_{FT})

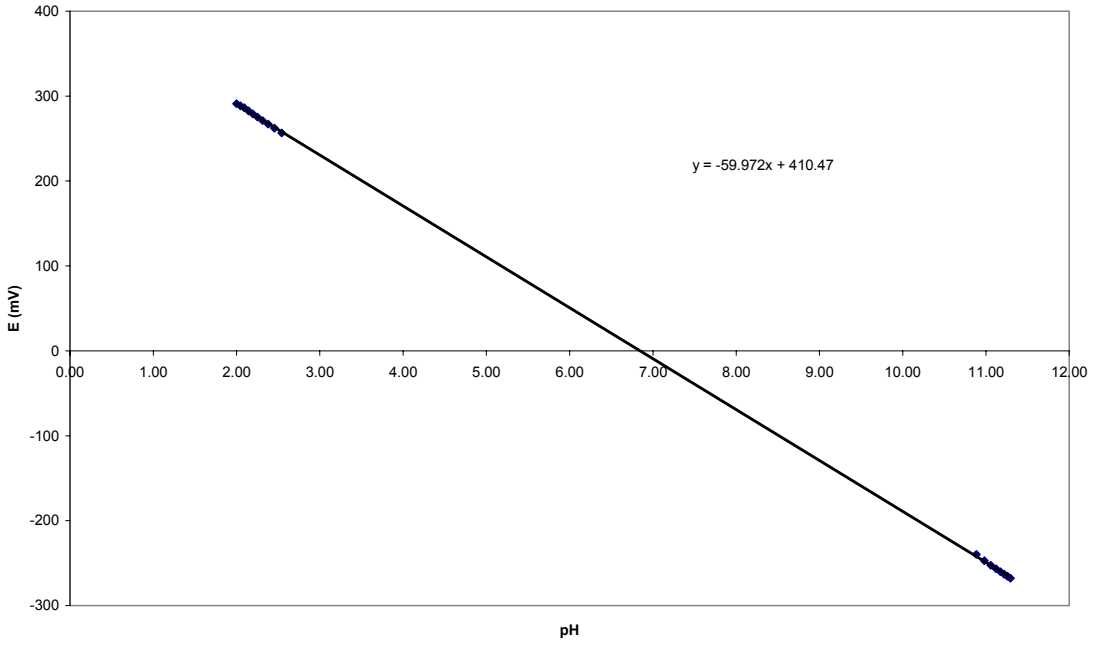

Figure 6: Plot of potential (E) in mV vs. pH for standardization titration

and protonated free ligand (L). The following series of equations derive the formulas used to calculate $\bar{n}$ (ratio of bound ligand to total metal concentration), as well as all species of ligand.

$$H_T = [H^+] + [HL] + 2[H_2L] + 3[H_3L] \quad (4)$$

Where H_T is the total acid added to the reaction, HL, H_2L and H_3L are all species of protonated ligand, in this case, PATH. Rearranging the equation gives

$$H_T - H^+ = [L]\{K_1[H^+] + 2\beta_2[H^+]^2 + 3\beta_3[H^+]^3\} \quad (5)$$

$$[L] = \frac{(H_T - H^+)}{(K_1[H^+] + 2\beta_2[H^+]^2 + 3\beta_3[H^+]^3)} \quad (6)$$

where β_1, β_2 and β_3 are the overall stability constants derived from the formation constant, K and $[H^+]$ is the free proton concentration measured by glass electrode potentiometry. From the pK_a's, the overall stability constants, β, can be calculated using the following equations:

$$\beta_1 = K_1 \quad (7)$$

$$\beta_2 = K_1K_2 \quad (8)$$

$$\beta_3 = K_1K_2K_3 \quad (9)$$

Once [L] is found, the complexed species of ligand (ML) must be calculated again with mass balance equations for the ligand. The free ligand (L_{FT}) may be calculated using the following equations

$$L_{FT} = L + LH + LH_2 + LH_3 \quad (10)$$

$$L_{FT} = L\{1 + K_1[H] + 2\beta_2[H]^2 + 3\beta_3[H]^3\} \quad (11)$$

Once both [L] and [L_{FT}] are known, the only species left is complexed metal-ligand species, ML. This may be solved with a simple difference equation

$$[ML] = L_T - L_{FT} \quad (12)$$

It can be assumed that all of the metal present in solution has been complexed with the ligand. This allows us to disregard complicated equations dealing with free metal in solution or metal complexes that form dimers with the ligand. The ratio of metal-ligand complex to the total concentration of metal ion is given as $\bar{n}$. This expression relates the extent of formation of a metal/ligand complex to metal ion concentration in solution. Using the following equations, an experimental and observed value of $\bar{n}$ may be calculated

$$\bar{n} = \frac{[ML]}{\text{total conc. of metal ion}} \text{ (experimental)} \quad (13)$$

$$\bar{n} = \beta_1[H^+] + 2\beta_2[H^+]^2 + 3\beta_3[H^+]^3 / 1 + \beta_1[H^+] + 2\beta_2[H^+]^2 + 3\beta_3[H^+]^3 \text{ (theoretical)} \quad (14)$$

In the case of cyclen, the $\bar{n}$ value obtained corresponds to a hydroxide complexed to the coordinated metal ion. Therefore, the free –OH in solution must be calculated. The equation for calculating this is given

$$\text{-OH (free)} = 10^{(pH - 13.78)} \quad (15)$$

Using this equation with the following

$$\bar{n}\,(OH) =$$

$$\frac{(\text{base added} \times \text{conc. base/total vol.}) - (\text{acid added} \times \text{conc. acid/total vol.}) + [H^+] - [OH^-]}{\text{total conc. of metal ion}} \quad (16)$$

will give the experimental value of $\bar{n}$ (OH). To calculate the theoretical $\bar{n}$ (OH), the following equation is used

$$\bar{n}\,(\mathrm{OH}) = \frac{1}{\left(\frac{1}{K_1(OH^-)}\right)+1} \qquad (17)$$

where $K_1(OH^-)$ is 6.19 for OH^-.

PATH Results

The plot in Figure 7 shows the plot of $\bar{n}$ vs. pH for PATH-H· $3HNO_3$. The potentiometric titration data was used to generate the plot. The three slopes in the graph correspond to the three pK_a's of PATH. The three pK_a's at 3.211, 6.998, and 10.501 correspond to the deprotonation of the terminal thiol group, the secondary amine and the pyridine group, respectively. The first protonation constant (log K = 10.501) is comparable to that of ethanethiol (log K = 10.61)[63]. There was considerable precipitate present above a pH of 11, which was concluded to be the hydroxide species. Using Eqs. 7, 8, and 9, the overall stability constants, β_1, β_2, and β_3 were found to be 3.17×10^{10}, 3.08×10^{17}, and 5.01×10^{20}, respectively. Substituting these values in to Eq. 18 yields the theoretical value for $\bar{n}$:

$$\bar{n} = \beta_1[H^+] + 2\beta_2[H^+]^2 + 3\beta_3[H^+]^3 / 1 + \beta_1[H^+] + 2\beta_2[H^+]^2 + 3\beta_3[H^+]^3 \qquad (18)$$

By plotting theoretical $\bar{n}$ vs. pH, an excellent correlation between experimental and theoretical data is shown (Figure 7). These pK_a values were used by Goldberg in his current research and publications.[51] Once the pK_a's of PATH were determined, focus was placed on observing PATH complexed with metal ions Pb^{2+}, Ni^{2+}, In^{3+}, and Zn^{2+}. These metal ions were selected due to their abundance and chemical significance in biological and biomedical systems.

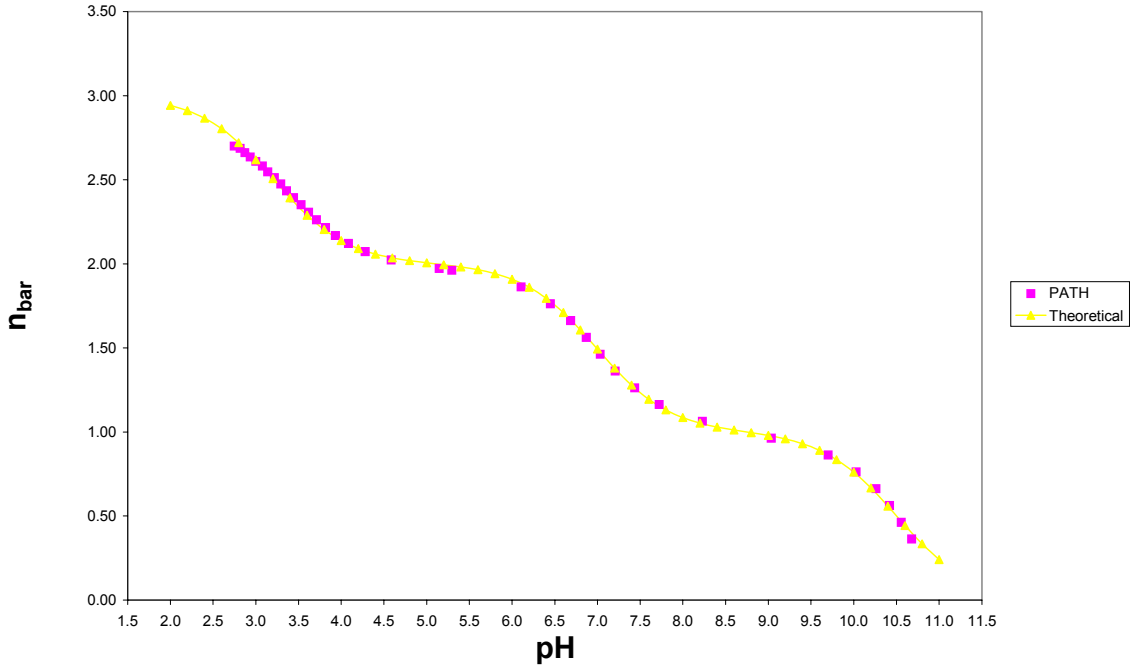

Figure 7: Plot of $\bar{n}$ vs pH for PATH-H

In Figure 8a, the titration data for PATH-H $3HNO_3$ in the presence of $Pb(NO_3)_2$ (1.75:1 PATH: Pb), shows the formation of a PATH-Pb complex. The rise in the graph above $\bar{n}$ =1 indicates the formation of a (PATH)PbOH complex from the deprotonation of a complexed water molecule. Beyond pH = 7.2, precipitation was observed in the form of a hydroxide complex, so that further data could not be collected. A plot of theoretical $\bar{n}$ is included in Figure 8. Again, there is agreement with experimental and theoretical data. In Figure 8b, the data shows that the Log K_1 (PbL) = 9.5, again with a rise in the curve above $\bar{n}$ = 1.0. This is also due to hydroxide complex formation, PbLOH. In Figures 9, 10 and 11, similar results of PATH complexed with Zn^{2+}, Ni^{2+} and In^{3+} are observed as with Pb^{2+}. All plots show a rise in $\bar{n}$ above 1.0 and correlate well with theoretical data. From this data, the log K values for PATH with each metal ion are given in Table 7. Figure 9a holds quite a bit of interesting information within it. The rise in the curve above $\bar{n}$ = 1.0 is the deprotonation of the coordinated water molecule on the (PATH)Zn complex, which is a pK_a = 7.7. To our knowledge this is the first time that a pK_a value has been found for a water molecule attached to a N_2S(thiolate)-Zn^{2+} center. As compared to related structures such as [12]aneN_3 (pK_a = 7.3)[26], this value is to be expected since PATH and [12]aneN_3 contain the same number of donor atoms. The increase of pK_a can be attributed to the thiolate donor group, which places electron density on the metal ion and causes a decrease in Lewis acidity. The pK_a values for PATH-M (M = Pb^{2+}, Ni^{2+}, In^{3+}) with a coordinated water molecule can been calculated from Figures 8b, 10b and 11b. The pK_a values for Pb^{2+}, Ni^{2+} and In^{3+} are found to be 6.8, 6.6 and 5.7, respectively. It has been pointed out by Goldberg[51] that adding a thiolate group onto a tridentate ligand has a similar effect on pK_a as adding a fourth nitrogen

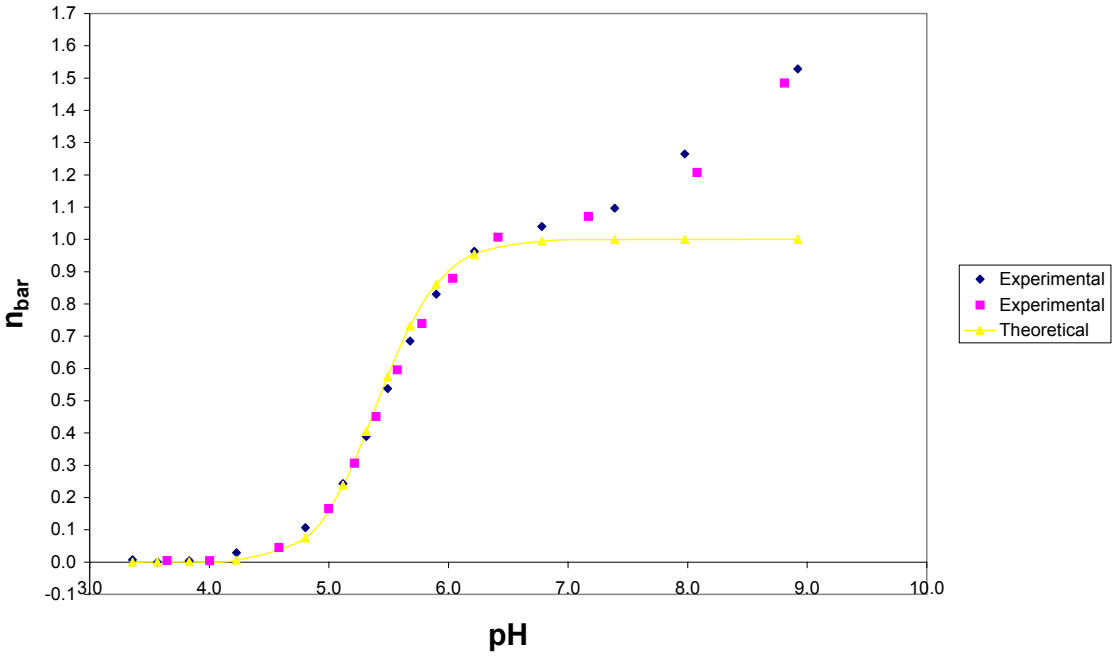

(a)

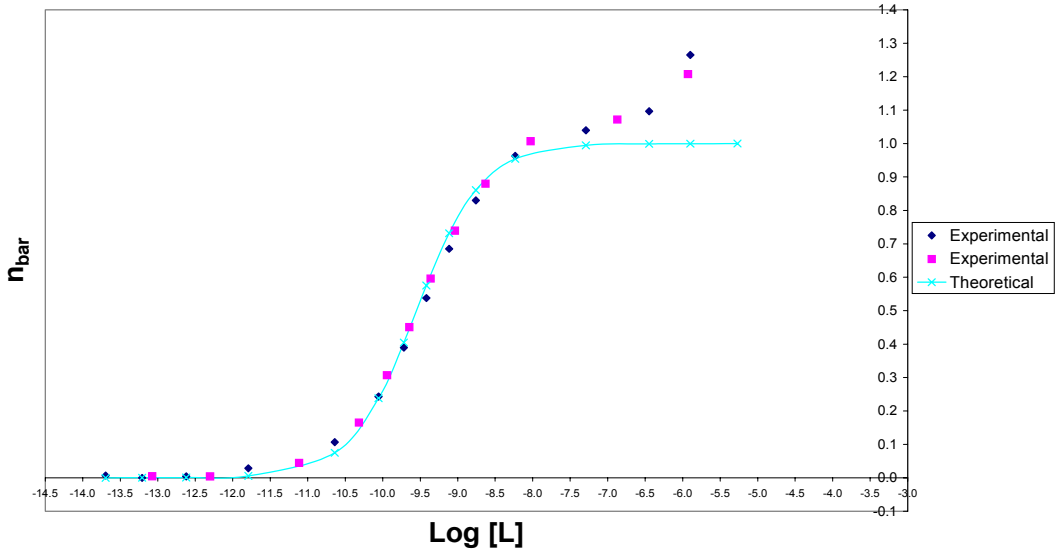

(b)

Figure 8: Plot of (a) $\bar{n}$ vs. pH and (b) $\bar{n}$ vs. Log [Pb^{2+}] for the PATH-Pb complex. The solid line in each graph represents the theoretical $\bar{n}$ curve, calculated from protonation constants and formation constants found in Table 7.

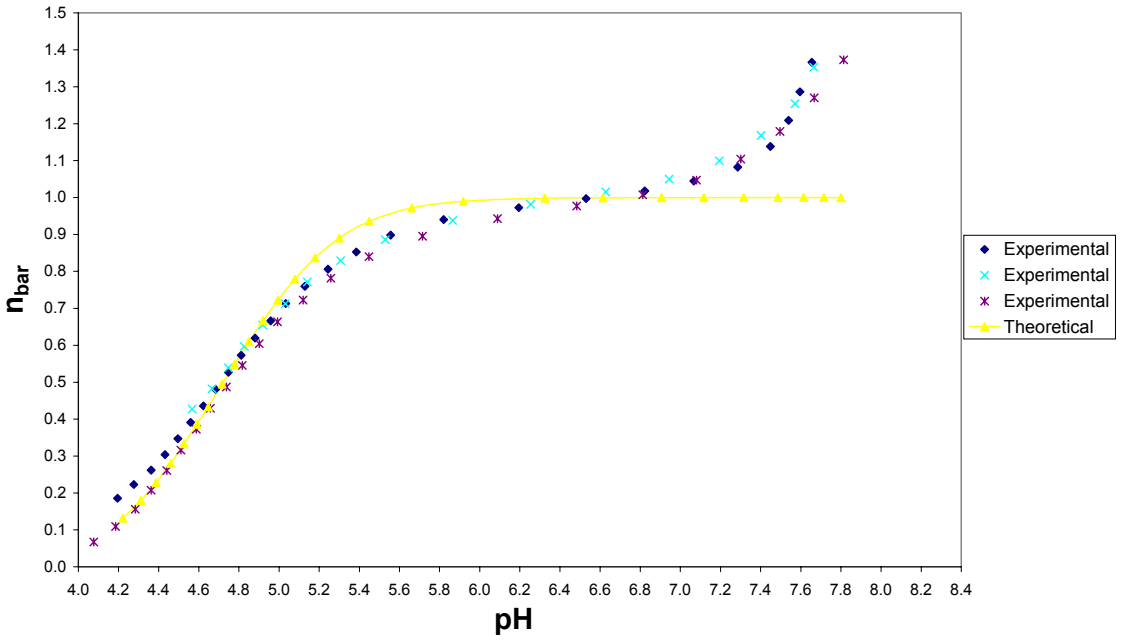

(a)

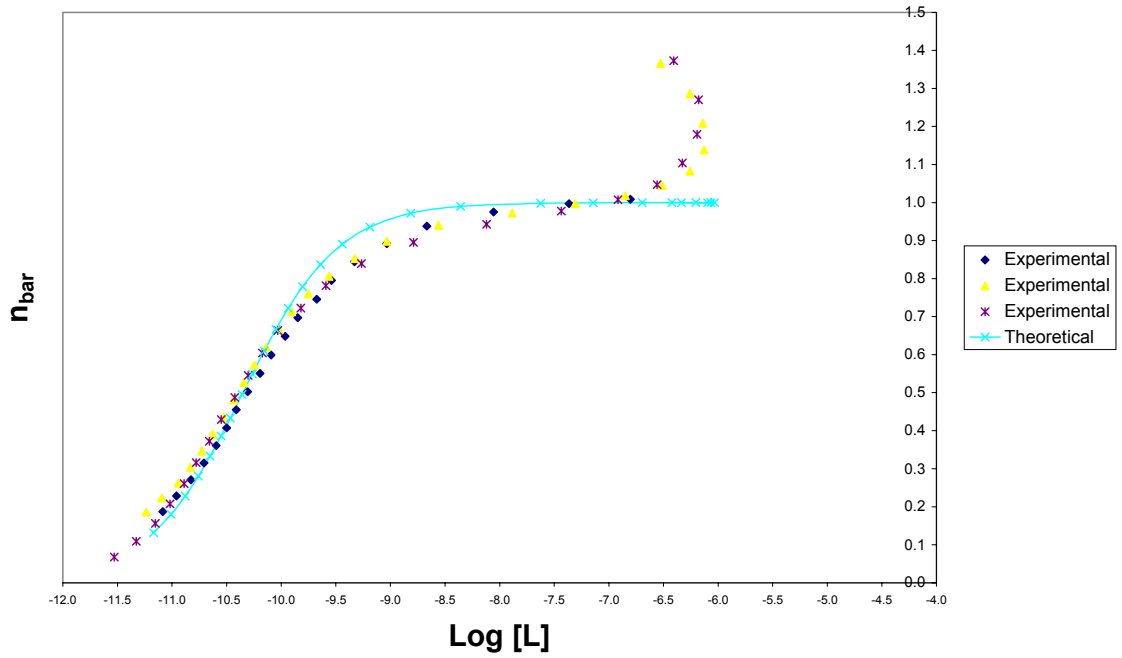

(b)

Figure 9: Plot of (a) $\bar{n}$ vs. pH and (b) $\bar{n}$ vs. Log [Zn^{2+}] for the PATH-Zn complex. The solid line in each graph represents the theoretical $\bar{n}$ curve, calculated from protonation constants and formation constants found in Table 7.

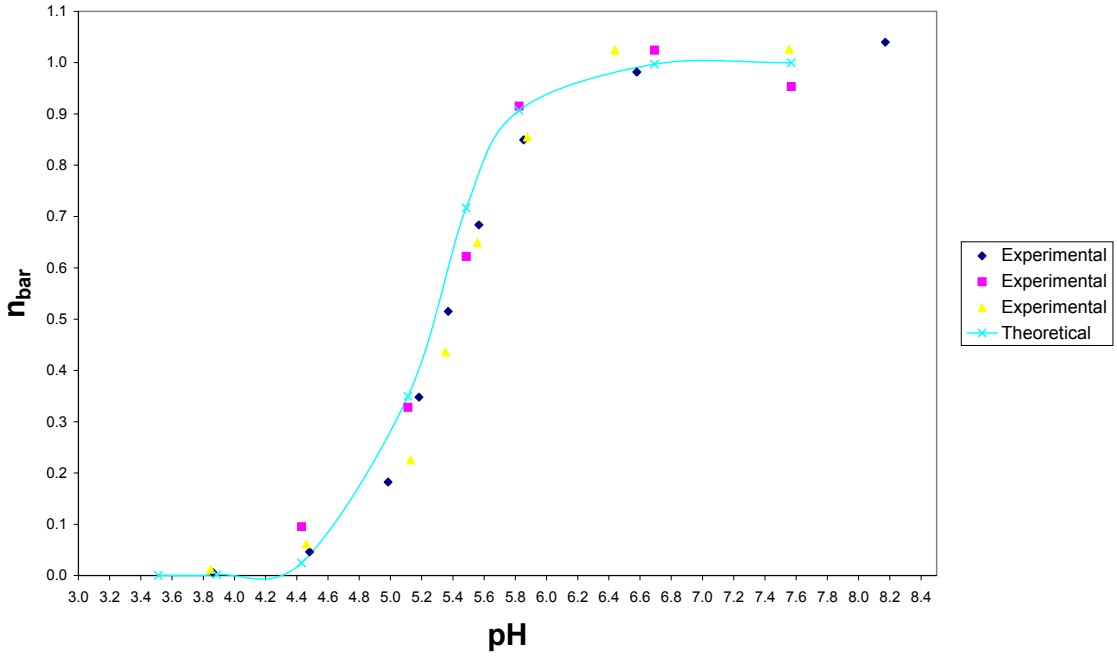

(a)

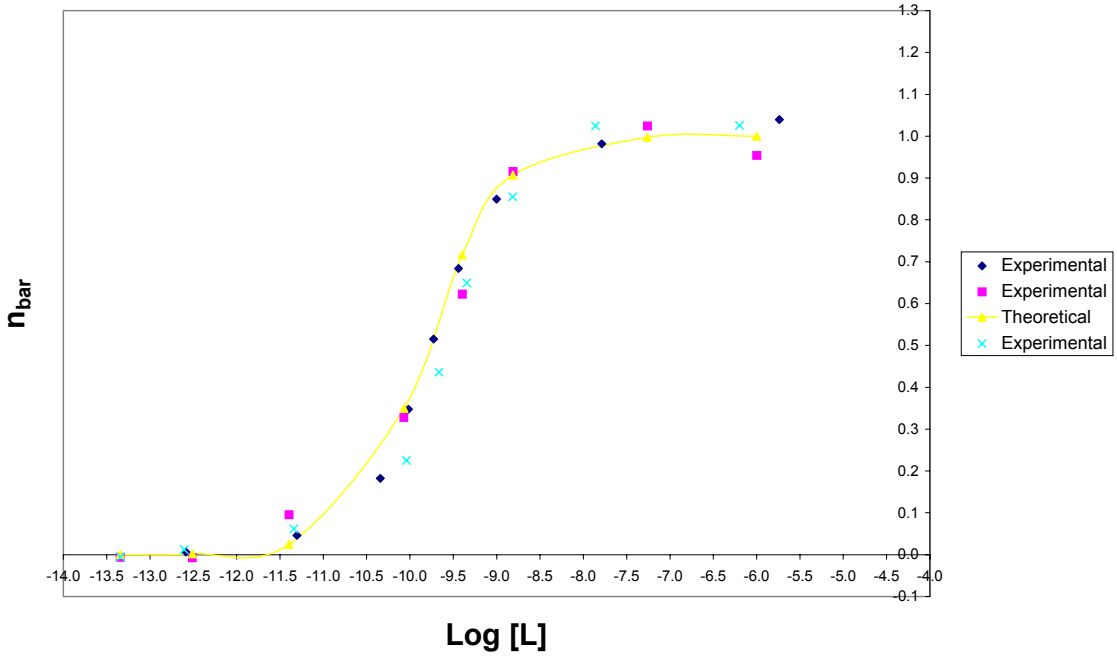

(b)

Figure 10: Plot of (a) $\bar{n}$ vs. pH and (b) $\bar{n}$ vs. Log [Ni^{2+}] for the PATH-Ni complex. The solid line in each graph represents the theoretical $\bar{n}$ curve, calculated from protonation constants and formation constants found in Table 7.

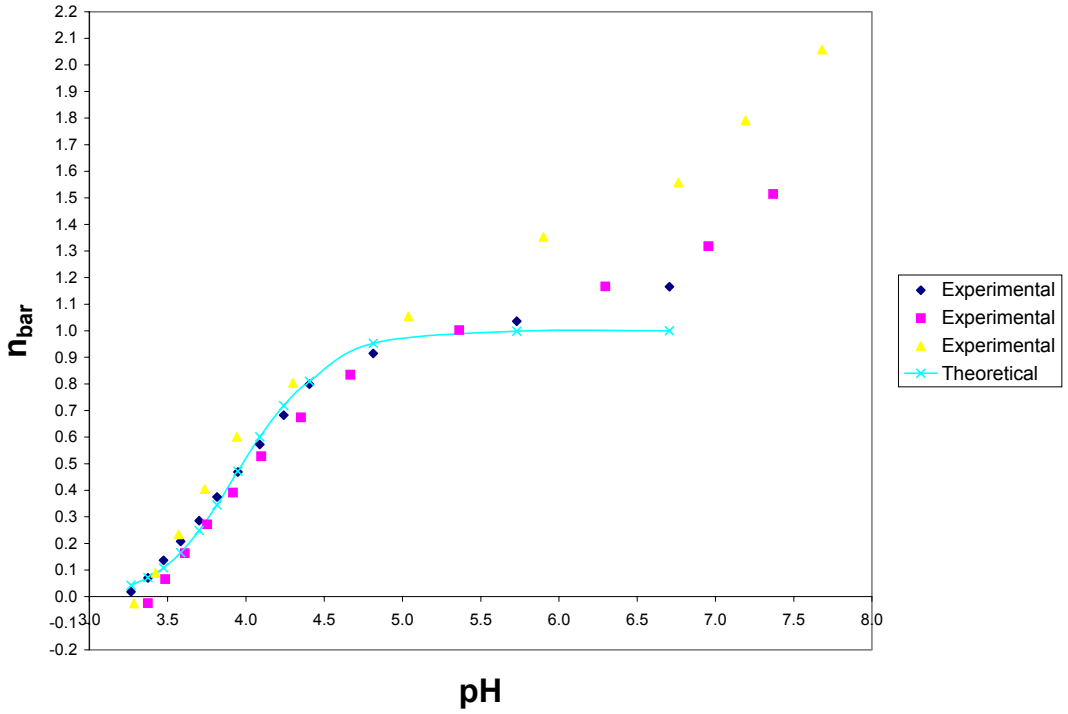

(a)

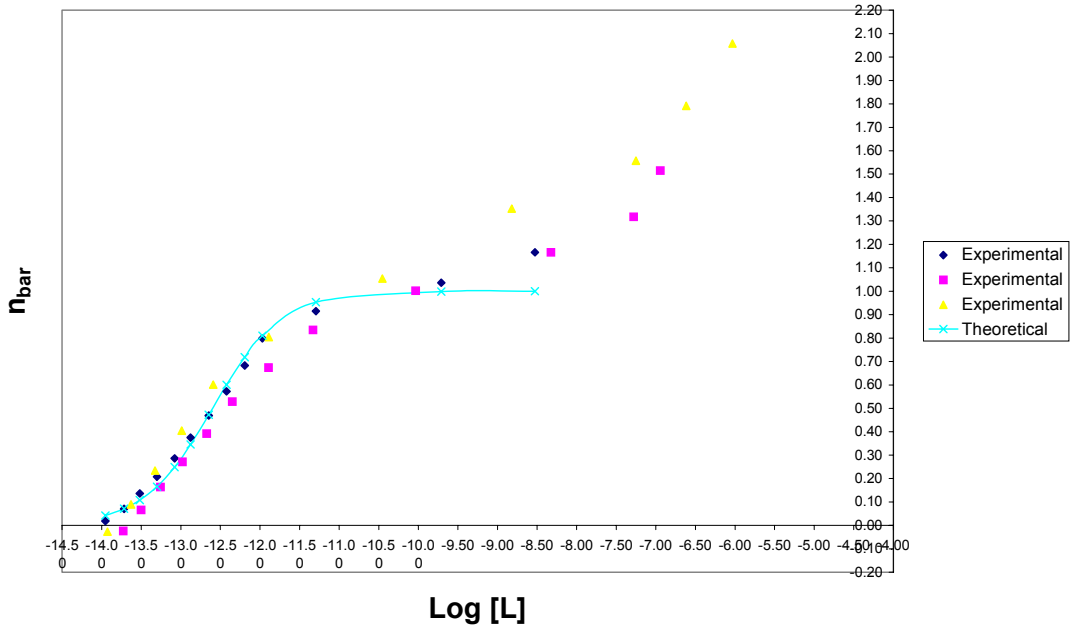

(b)

Figure 11: Plot of (a) $\bar{n}$ vs. pH and (b) $\bar{n}$ vs. Log [In^{3+}] for the PATH-In complex. The solid line in each graph represents the theoretical $\bar{n}$ curve, calculated from protonation constants and formation constants found in Table 7.

Table 7: Log K_1 values for PATH-M complex (M = Pb^{2+}, Zn^{2+}, Ni^{2+}, In^{3+})

Metal ion	Log K_1
Pb^{2+}	9.5
Zn^{2+}	10.3
Ni^{2+}	9.7
In^{3+}	12.4

donor atom. However, it was thought that the thiolate group would donate electron density and therefore decrease the acidity of the coordinated water molecule. Given the present data, adding the thiolate group does not decrease the acidity of the coordinated water molecule, giving a pH of 9 or higher as hypothesized. As these are important factors in determining pK_a, other factors not yet dealt with must be taken into account. To date, there is little experimental data to support purely theoretical data on the effects of coordination number and donor type on the pK_a of zinc model enzymes. This preliminary work with a N_2S (thiolate) MOH complex is the first step in providing insight into this area.

As mentioned previously, voltammetry was also employed as an analytical tool for the observation of species in solution. Using the mercury electrode, reduction of species in solution takes place and, depending on the type of species present, reduction peaks may appear for each species. In addition, as the pH of the reaction solution is increased the potential for each peak shifts to a more negative potential. By plotting the peak potential as a function of pH, we can gather information about the species present in the reaction solution. It is known that the slope of the peak potential as a function of pH indicates the number of protons involved in the reduction process. In Figure 5, it is shown that a slope of 59.16 mV/decade indicates 2 protons involved in the reduction process, while a slope of 29.58 mV/decade indicates one proton involved in the reduction process. It is also shown that pK_a values may be found by changes in the slope of the plot. Figure 12 shows the differential pulse polarograms for the PATH-Zn complex with increasing pH. It is concluded that the $[Zn(PATH)OH_2]^+$ complex appears at a potential of -1.2 V and a pH of about 5.6. The peak continues to become more defined and

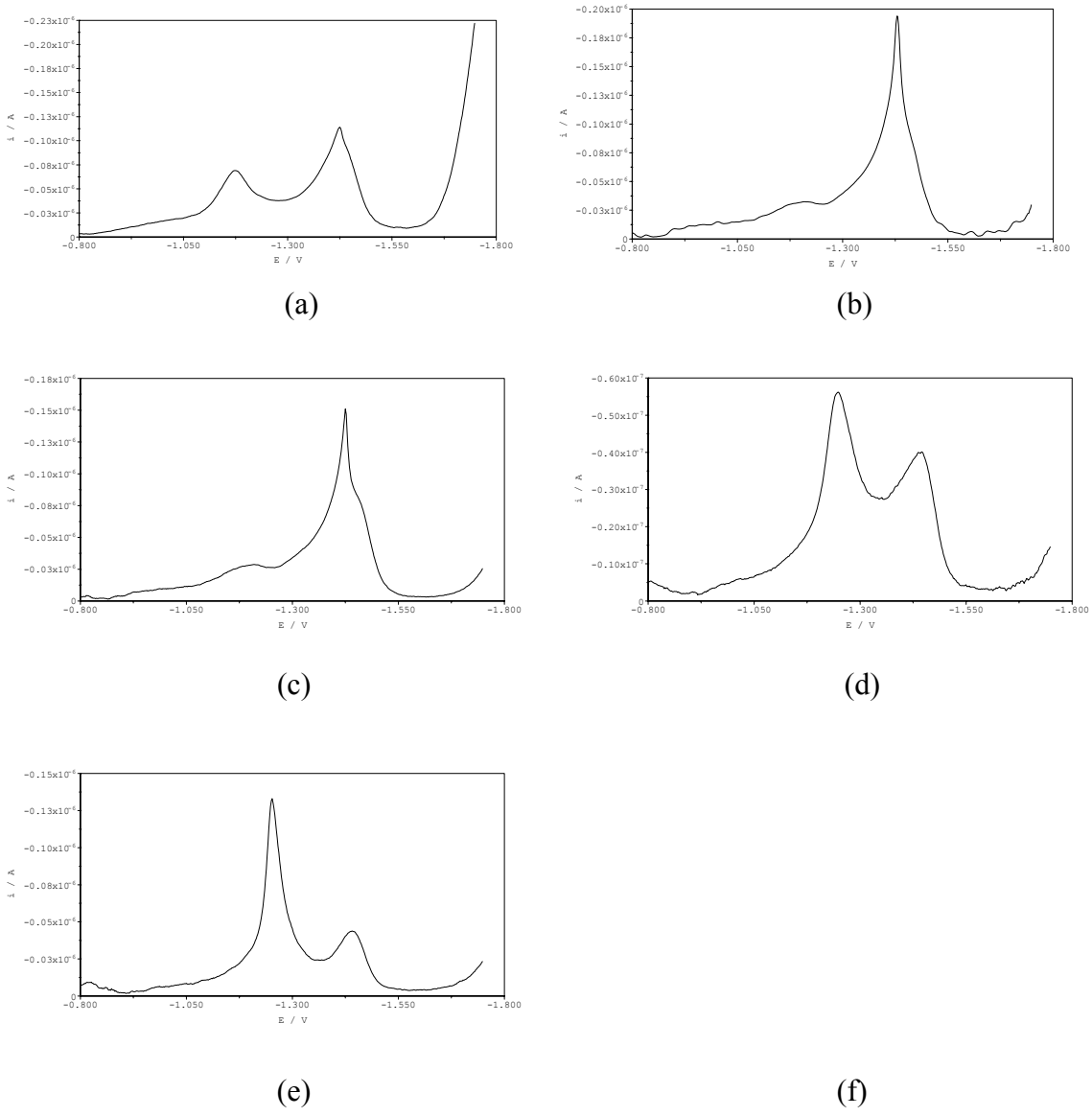

Figure 12: Differential pulse polarograms [(a) to (f)] for PATH-Zn complex as a function of pH. The pH values of each polarogram are as follows: (a) 5.623, (b) 6.723, (c) 8.055, (d) 9.088, (e) 10.074, (f) 11.011

increases in height as the pH is increased. At pH 9.1 (Figure 12(d)), the peak is well defined, which indicates an equilibrium between $[Zn(PATH)OH_2]^+$ and [Zn(PATH)OH]. At pH 10 and above, the peak becomes sharp and well separated from the other peak, assumed to be the reduction of the proton. Figure 13 shows the shift in peak potential (E) in V as a function of pH. Each data point represents the peak potential of the PATH-Zn complex. The first rise in the graph occurs at about pH 4.5 and indicates the reduction of $[Zn(PATH)OH_2]^+$ complex with the use of 2 protons to give a slope of 60 mV/decade. As mentioned before, the involvement of 2 protons is confirmed by the slope close to the Nernstian slope. As the complex becomes reduced, the Zn(II) ion becomes amalgamated by the mercury electrode. There is a second shift to more negative potential in the graph, where there are two slopes of 60 mV/decade and 30 mV/decade. The slope of 60 mV/decade as mentioned previously corresponds to the involvement of 2 protons in the reduction of [Zn(PATH)OH] to PATH-H. The slope of 30 mV/decade corresponds to the involvement of 1 proton in the reduction of [Zn(PATH)OH] to $PATH^-$. With the use of differential pulse polarography, we are able to see two reduced species of $[Zn(PATH)OH_2]^+$ where as with potentiometry this would not have been possible.

It was thought that polarography would not have been a valid analytical technique for researching the ligand PATH due to the thiolate group present. Since the thiolate group tends to bind mercury quite strongly, we feared there would be a complexation problem with the ligand and the mercury electrode, hence generating inaccurate data. Certain measures were taken to ensure that this did not become a significant problem. The reaction solution was not in contact with the electrode longer than needed, only being in contact with the electrode during the course of the experiment. This seemed to

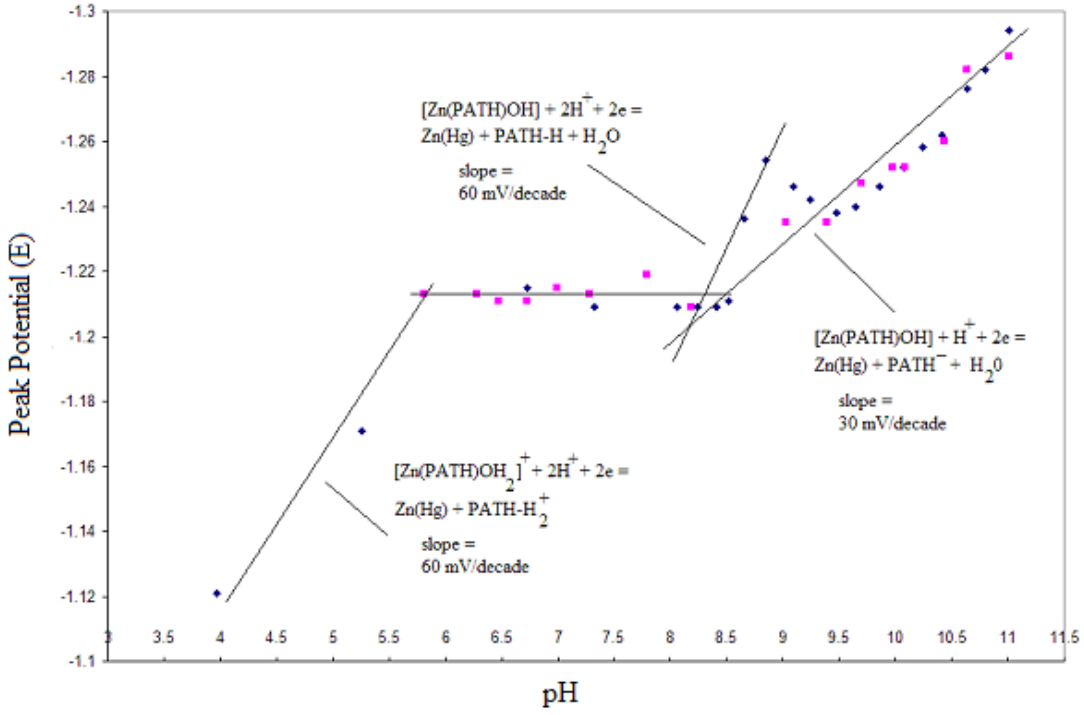

Figure 13: Plot of peak potential (E) as a function of pH for the Zn(PATH) complex.

limit coordination of the thiolate on the PATH ligand to the mercury electrode. A second, possibly more important precaution was not to scan at less negative potentials than absolutely necessary, since the more positive the potentials, the more likely this was to lead to oxidation of Hg in the presence of ligands. Once we were reassured that polarography of the PATH ligand was possible, our focus turned to study PATH with the very acidic metal ion Bi^{3+}, which can usually only be studied with polarography. From the information gathered, we were able to deduce the presence of the reduction of Bi^{3+} and the PATH-Bi complex.

Cyclen Results from Glass Electrode Potentiometry.

From a titration of protonated cyclen with standardized base, the pK_a values for cyclen (log K = 10.65, 9.64 and 1.4) were found. Using Eqs. 7, 8 and 9, the overall protonation constants, β_1, β_2, and β_3, were found to be 4.47×10^{10}, 1.95×10^{20} and 4.90×10^{21}. In all titrations for cyclen, zinc was complexed initially, followed by coordination of ligands onto the complexed metal ion. Figure 14 shows the plot of $\bar{n}$ as a function of pH for the cyclen-Zn complex. In this case, $\bar{n}$ represents the number of bound hydroxides to the complexed metal ion rather than the ratio of metal-ligand complex to total metal ion concentration. This is to say that we are measuring ligands being displaced by competing hydroxides being bound. As the pH of the reaction solution is raised, hydroxides are competing with already bound ligands to the cyclen-Zn complex. Since hydroxides bind more strongly to the metal-ligand complex than most other ligands, displacement of bound ligands is inevitable and this degree of

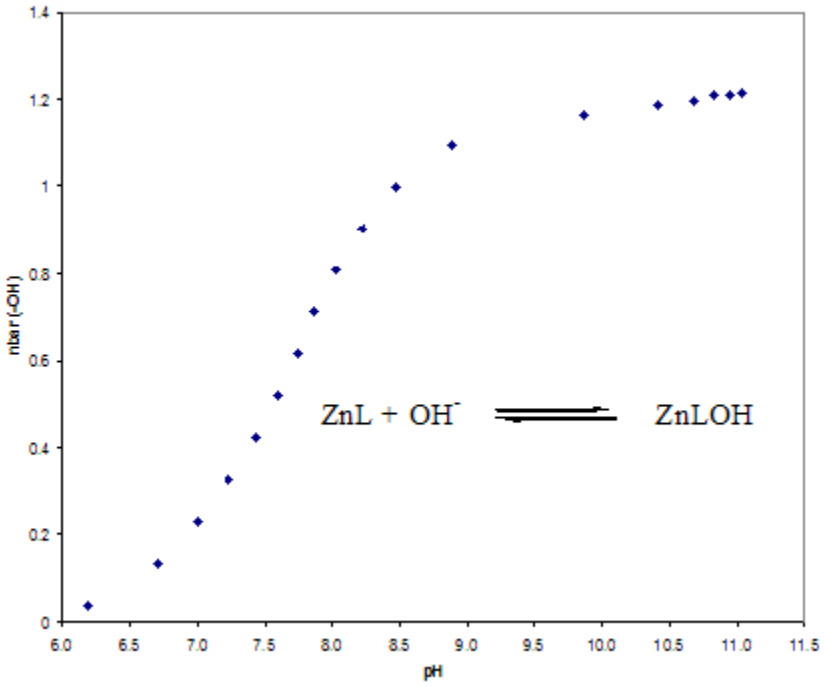

Figure 14: Plot of $\bar{n}$ ($^{-}$OH) as a function of pH for the cyclen-Zn complex

displacement may be measured. This gives us a direct method of measuring various ligands being bound to the complexed metal ion.

In aqueous solution, the Zn(PATH) complex contains two bound water molecules. Displacement of one of these aquo ions causes a shift in the potential of the electrochemical cell. This shift can be observed as a function of the pH of the solution. Depending on the kinetics and thermodynamics of the ligand being bound to the metal-ligand complex, the plot of $\bar{n}$ (OH^-) vs. pH will shift relative to the plot of the cyclen-Zn complex with no metal ions attached. If the complex is relatively strong, the shift will be considerably bigger than if the complex is relatively weak. From these shifts, formation constants can be calculated for each cyclen-Zn-L complex (L = triphenylphosphine, Cl^-, Br^-, I^-, thiourea, CN^-, thiocyanate, azide). These ligands were selected due to their varying size, steric hindrance and ability to complex. Triphenylphosphine is a rather sterically hindered ligand which makes complexation difficult. However, we have shown that the geometry and orientation of the cyclen-Zn complex allows the ligand to bind where before it was not possible. The ligands Cl^-, Br^- and I^- are commonly used in research since they provide information on electronegativity and size restrictions. Thiourea, CN^-, thiocyanate and azide are all known to form relatively stable complexes with a variety of ligands. This allows for valuable data to be obtained with a diverse group of ligands.

The first ligand that shows a shift in its $\bar{n}$ (OH^-) vs. pH plot is thiourea (Figure 15). As can be seen from the graph, there is a small shift in the curve due to the formation of the cyclen-Zn-thiourea complex. From this shift, a formation constant can

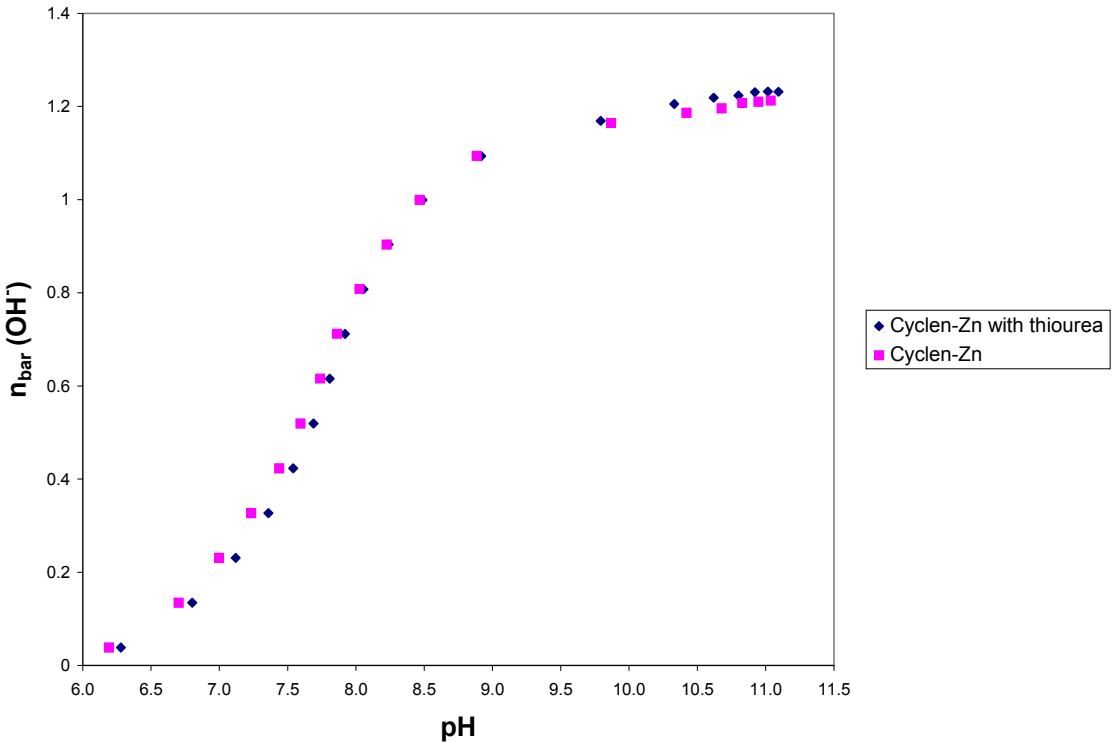

Figure 15: Plot of $\overline{n}$ ($^{-}$OH) as a function of pH for cyclen-Zn-thiourea complex. The rise in the graph above $\overline{n}$ =1 is due to hydroxide complex formation.

be calculated for the cyclen-Zn-thiourea complex. Eq. 18 gives the equation for calculating log K given a displacement in pH and concentration of ligand (L).

$$\log K = disp.in\ pH - \log[L] \tag{18}$$

Figures 16-20 show the same type of displacement of the plot of $\bar{n}$ (OH^-) vs. pH for triphenylphosphine (TPP), I^-, Br^-, Cl^- and CN^-, respectively. Figure 21 shows all ligands bound with the cyclen-Zn complex along with the cyclen-Zn complex with no additional ligands bound. In Figure 16, there is a shift in the $\bar{n}$ (^-OH) vs. pH plot which indicates the formation of a cyclen-Zn-TPP complex. This is quite a remarkable finding given the high level of steric hindrance of the TPP ligand (Table 8). The drop in coordination number from 6 in the aquo ion to 4 in the cyclen-Zn complex allows the TPP ligand to bind. However, the geometry of the complex is not the only factor that allows the TPP ligand to form a stable complex. An increase in Lewis acidity of the complexed zinc ion is also a benefit of a drop in coordination number. This increase in acidity is evident in the strong complexes of cyclen-Zn with the ligands found in Figure 21. In Figures 17-19, there is a gradual increase in the shift of the $\bar{n}$ (OH^-) vs. pH plot for the ligands I^-, Br^- and Cl^-. It is clear that the trend in Log K_1 follows: $I^- < Br^- < Cl^-$. In Figure 20, there is a large shift in the plot for the CN^- ligand. This large shift is to be expected since CN^- is known to bind strongly and form stable complexes in aqueous solution.

The trends found in Figures 17-19 are of great importance in relation to the HSAB theory of Pearson. This trend is the opposite of what Kimura discovered by complexing the zinc ion with 12-aneN_3. Kimura found log K values for I^-, Br^- and F^- to be 1.6 ± 0.1, 1.5 ± 0.1 and 0.8 ± 0.1, respectively.[50] The trend of log K values that Kimura obtained is opposite to that obtained in this work (Table 8). The fact that the ligands bind more

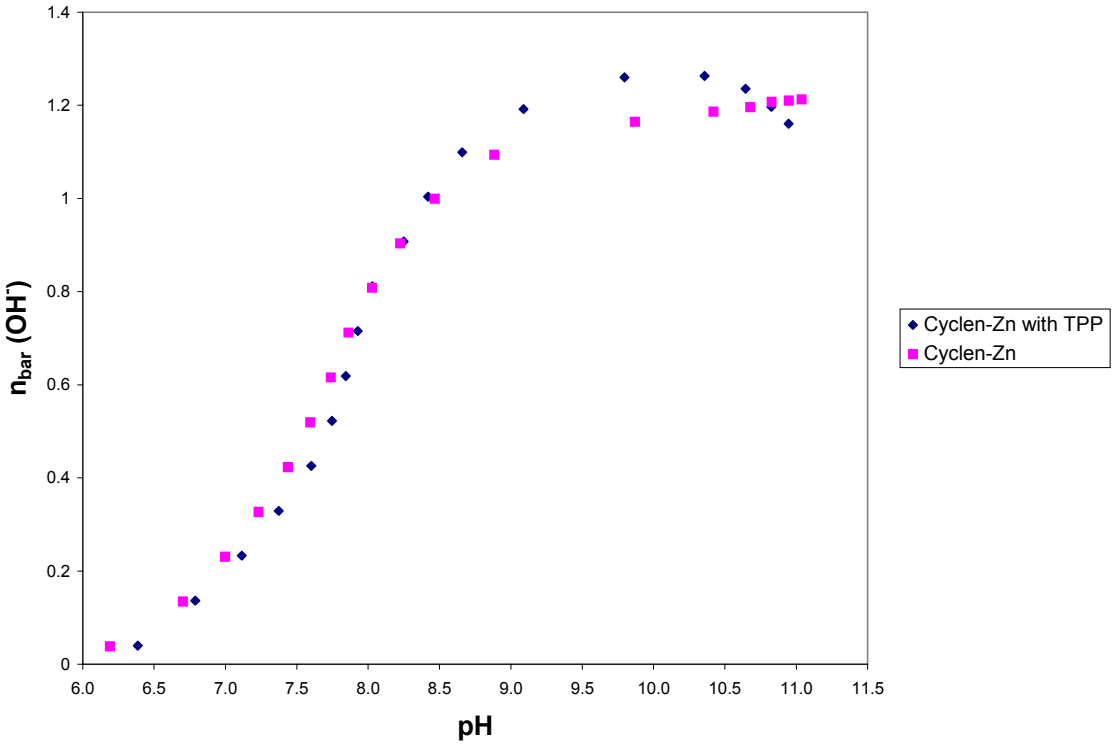

Figure 16: Plot of $\bar{n}$ ($^{-}$OH) as a function of pH for cyclen-Zn-TPP complex. The rise in the graph above $\bar{n}$ =1 is due to hydroxide complex formation.

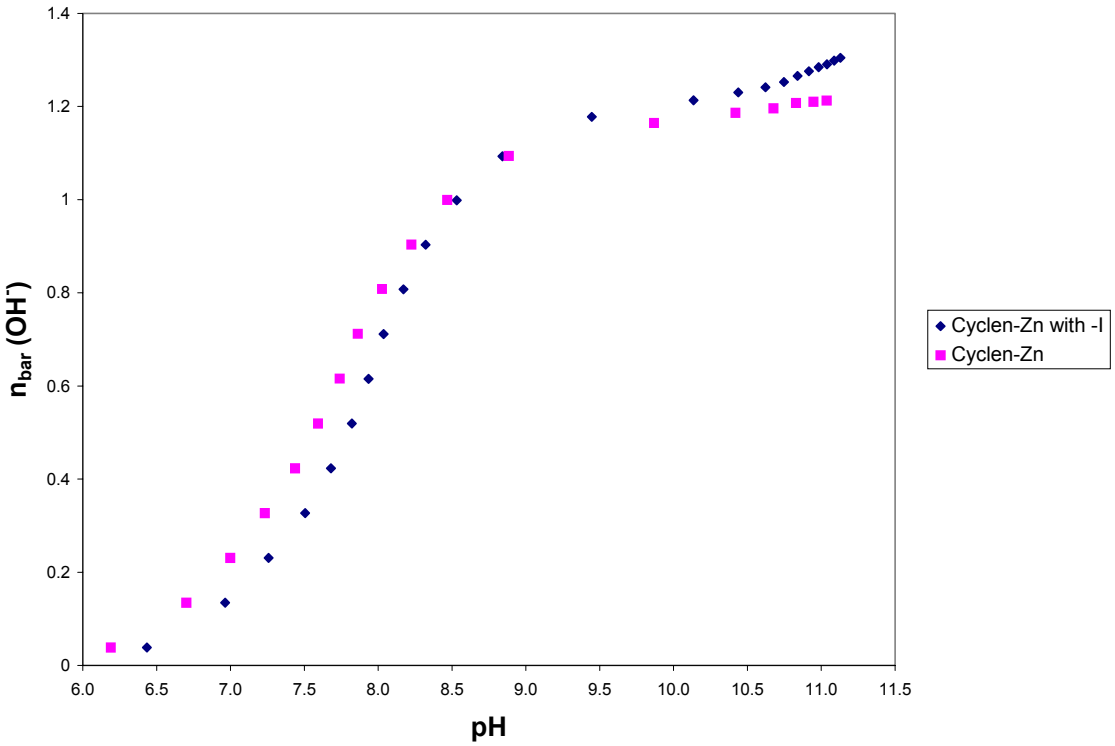

Figure 17: Plot of $\overline{n}$ ($^{-}$OH) as a function of pH for cyclen-Zn-I complex. The rise in the graph above $\overline{n}$ =1 is due to hydroxide complex formation.

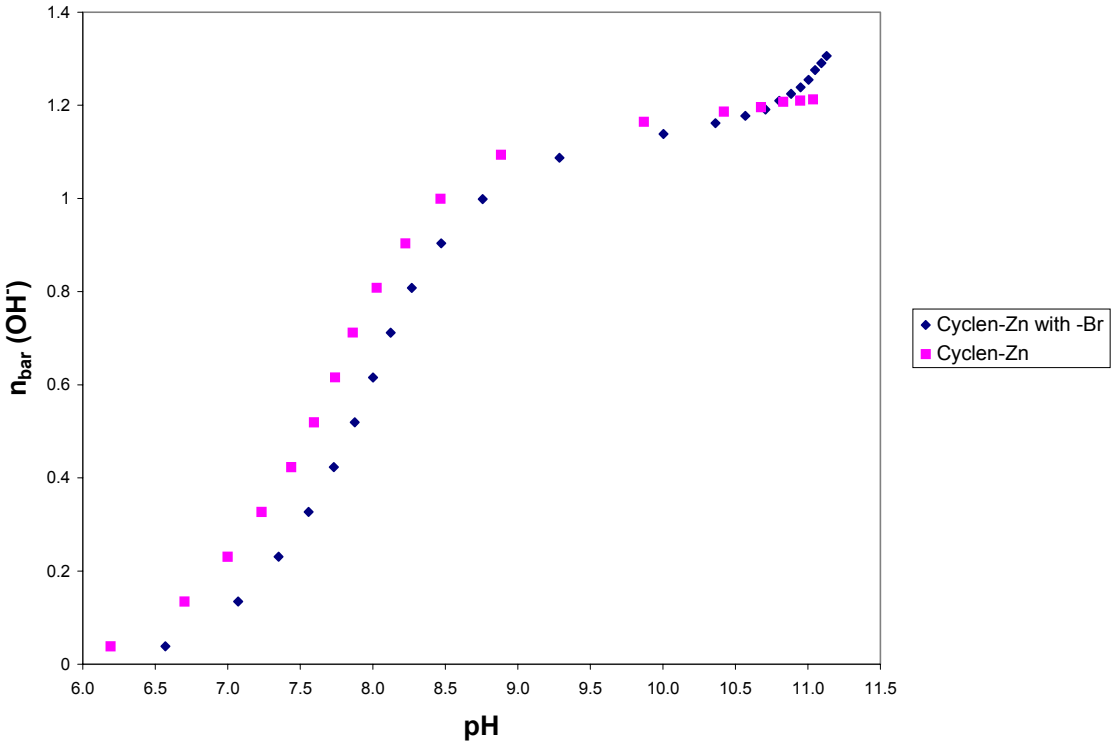

Figure 18: Plot of $\bar{n}$ ($^-$OH) as a function of pH for cyclen-Zn-Br complex. The rise in the graph above $\bar{n}$ =1 is due to hydroxide complex formation.

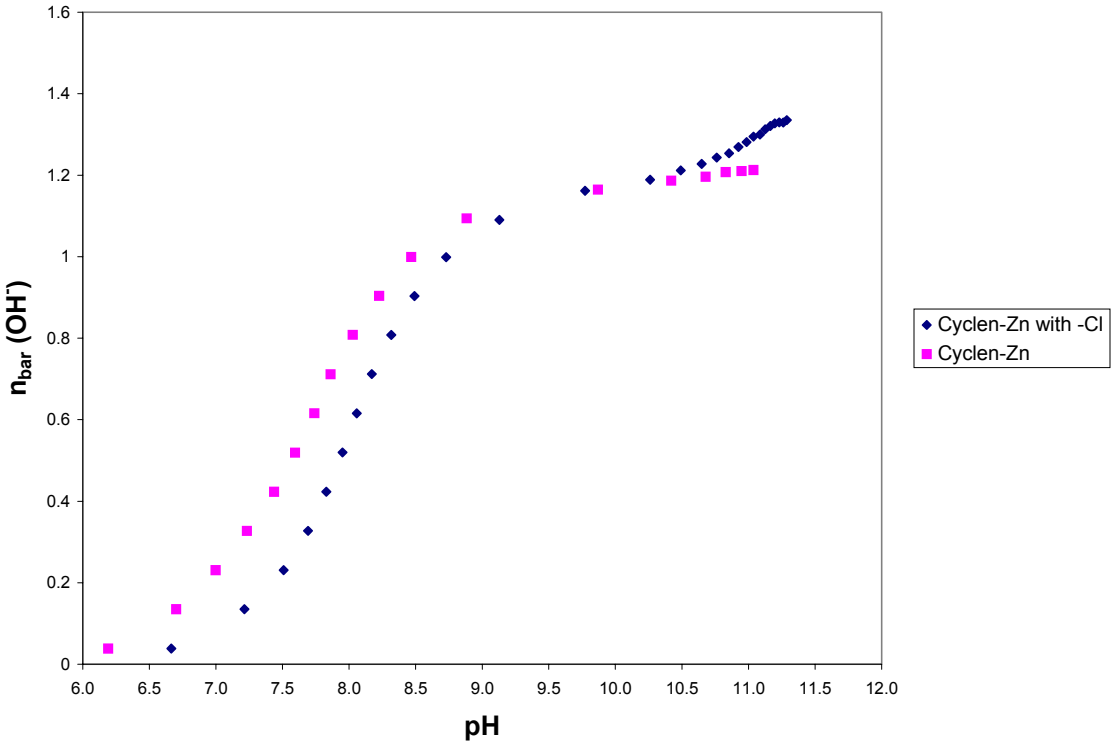

Figure 19: Plot of $\bar{n}$ ($^{-}$OH) as a function of pH for cyclen-Zn-Cl complex. The rise in the graph above $\bar{n}$ =1 is due to hydroxide complex formation.

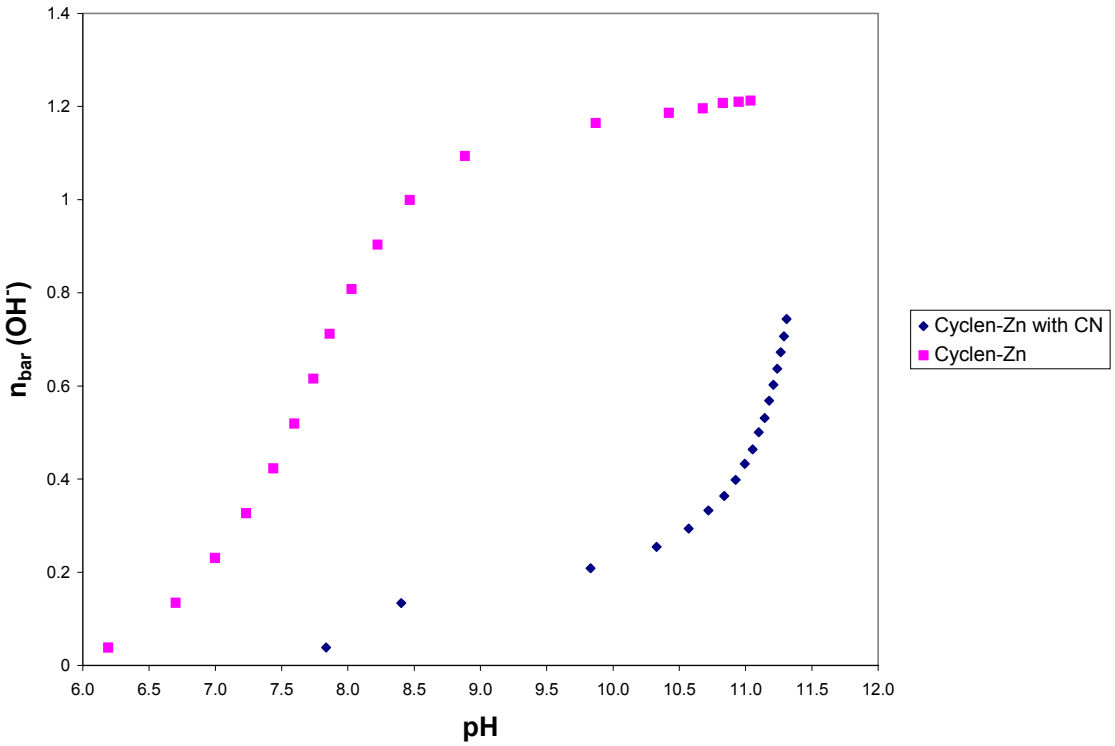

Figure 20: Plot of $\overline{n}$ ($^-$OH) as a function of pH for cyclen-Zn-CN complex. The rise in the graph above $\overline{n}$ =1 is due to hydroxide complex formation.

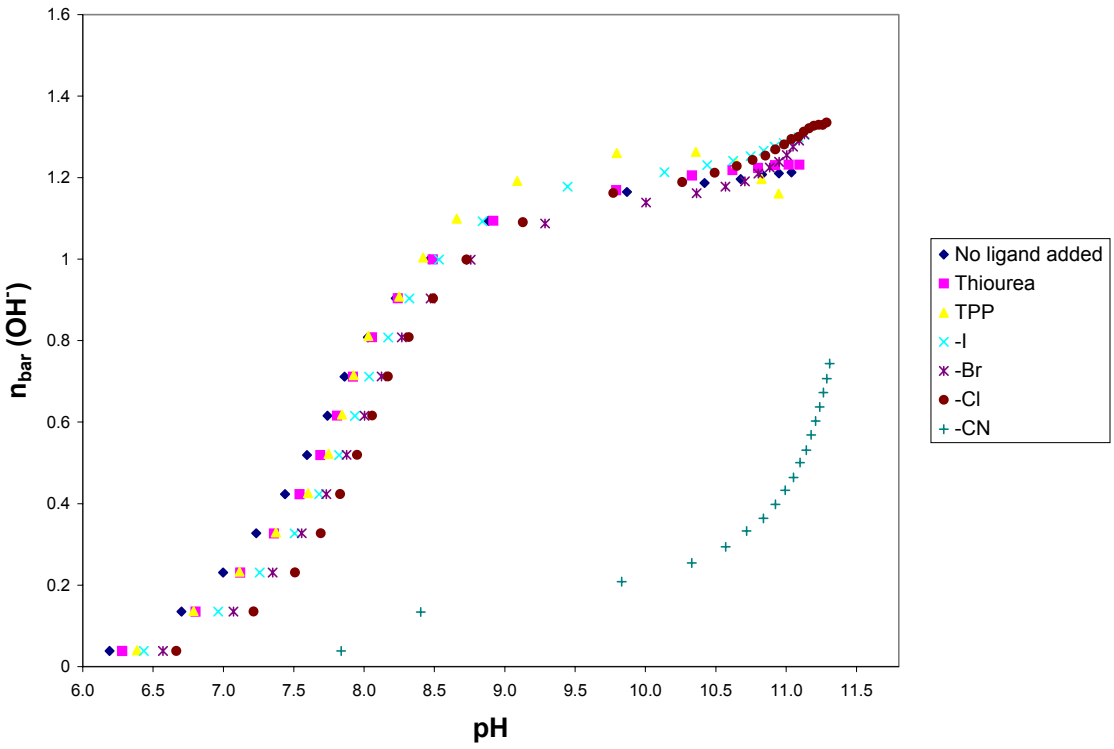

Figure 21: Plot of $\bar{n}$ ($^{-}$OH) as a function of pH for cyclen-Zn complex with all ligands. The rise in the graph above $\bar{n}$ =1 is due to hydroxide complex formation.

Table 8: Log of formation constants of ligands with cyclen-Zn complex

Ligand	log K_1
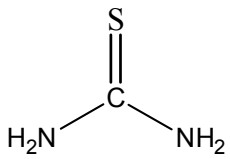	0.50
I^-	1.11
Br^-	1.44
Cl^-	1.67
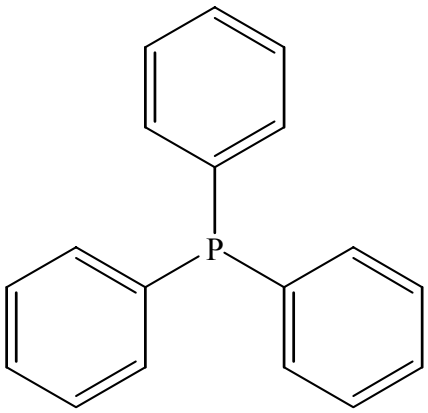	2.05
CN^-	4.37
OH^-	6.19

strongly and in an opposite trend in 12-aneN_3 than in cyclen indicates that the 12-aneN_3 affords a 'softer' Zn(II) ion than cyclen. The 4-coordinate nature of the 12-aneN_3 allows for the higher log K values for the ligands previously mentioned over cyclen, which is 5-coordinate. Table 8 shows the formation constants for thiourea, I^-, Br^-, Cl^-, TPP, CN^- and OH^- with the cyclen-Zn complex. These log K values were found using Eq. 18. These values correspond well to the plots of $\bar{n}$ ($^-$OH) vs. pH for all ligands with the cyclen-Zn complex. The relatively large formation constants indicate an increase in Lewis acidity of the complexed Zn(II) ion. The stronger acidity of the complexed Zn(II) ion increases the acidity of the coordinated water molecule when in an aqueous environment. This observation is substantiated with X-ray crystal structures obtained for the complexes Zn(cyclen)-thiourea (Figure 22) and Zn(cyclen)-I (Figure 23). Figures 22 and 23 also contain conformationally-optimized structures of the complexes, which are similar structures to those obtained with X-ray crystallography. These crystal structures show a distorted square pyramidal geometry of the Zn(cyclen) complex with the Zn(II) metal ion positioned out of the coordination sphere. This distortion was hypothesized to allow bulky donor ligands to bind to the complex. The bond lengths for each ligand complexed to the bound zinc metal ion are considerably longer than any other bonds in the structures. The Zn-S bond length in Figure 22 is 2.3128 Å, with the bond lengths for Zn-N1A, Zn-N2A, Zn-N3A and Zn-N4A are 2.233(6) Å, 2.191(6) Å, 2.084(6) Å and 2.136(7) Å, respectively. These bond lengths indicate a distortion from the otherwise tetrahedral geometry of the Zn(cyclen) complex in aqueous solution. The same can be seen for the Zn(cyclen)-I structure (Figure 23). The increase in lengths of the Zn-I and the 4 Zn-N bonds also indicate a distorted geometry. These crystals were also submitted

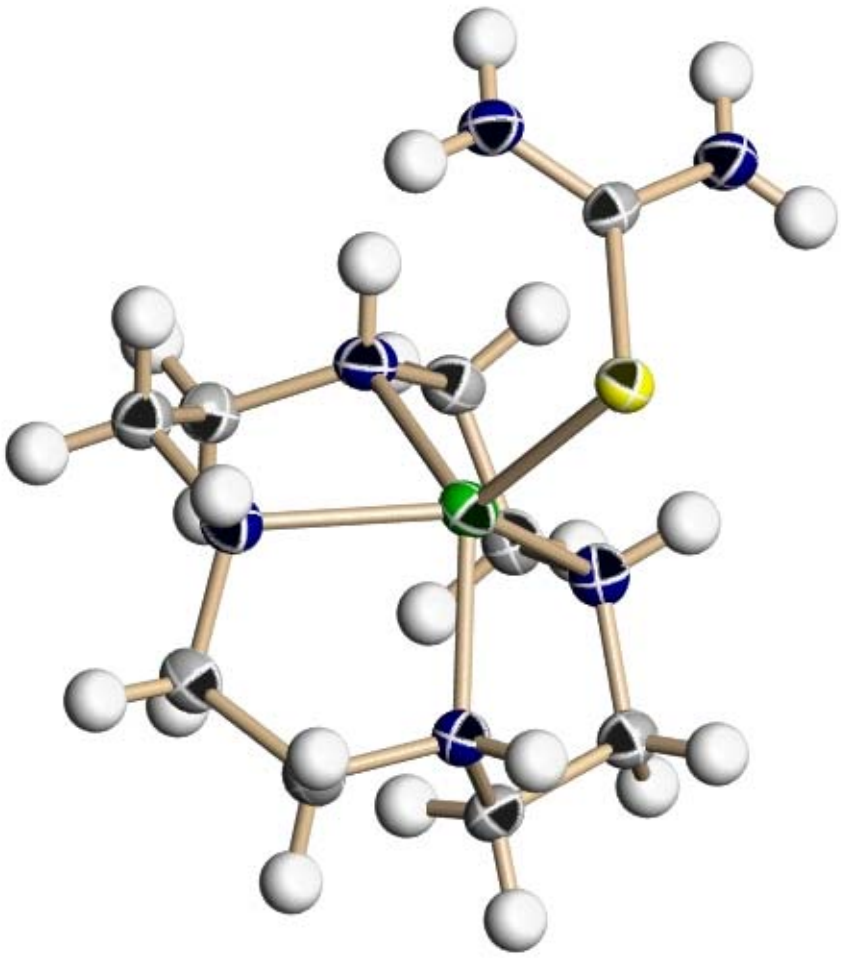

Figure 22: X-ray crystal structure for the Zn(cyclen)-thiourea complex.

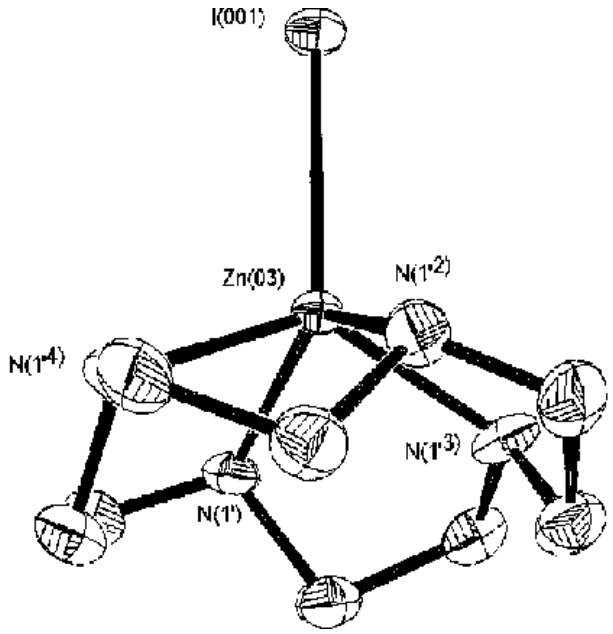

Figure 23: X-ray crystal structure of the Zn(cyclen)-I complex.

for C, H and N analysis. The Zn(cyclen)-thiourea results are as follows: Found: 24.85% C, 5.48% H, and 25.73% N, Calculated: 24.69% C, 5.53% H, and 25.60% N. The Zn(cyclen)-I results are as follows: Found: 22.46% C, 4.72% H, and 16.30% N, Calculated: 22.53% C, 4.73% H, and 16.42% N.

Voltammetry was used to analyze the acidity of the water molecules coordinated to the Zn(cyclen) complex. Figure 24 shows the appearance of a Zn(II) metal ion peak at -0.992 mV and a Zn(cyclen) complex peak at -1.323 mV, both appearing at a pH of 4.47. The position of the metal ion peak and complex peak is consistent with previous findings. The peaks that appear at -0.3 mV and -0.5 mV are due to the interference of the mercury electrode. There is also a peak that appears above -1.5 mV which is due to the reduction of the solvent. The peaks present in Figure 24 show the constant presence of the metal ion as well as the complex. However, there is a shift to a more negative potential as noted by peak position. Figure 25 shows the shift in peak potential (E) in V as a function of pH for the Zn(cyclen) complex. Similar results were found for the Zn(cyclen) complex as with the PATH-Zn complex. There is a shift in peak position which corresponds to the reduction of Zn(cyclen)OH_2 to Zn(cyclen)OH with 2 protons involved in the reduction process. As with the PATH-Zn complex, there are two reduced species which correspond to the involvement of one proton and two protons, which are indicated by the slopes of 30 mV/decade and 60 mV/decade, respectively. In addition to detecting two reduced species where otherwise would not have been detected, the intercept of the slope of each reduced species indicates the pK_a of the Zn(cyclen) complex. This pK_a of 8.6 corresponds very well to the pK_a for the Zn(cyclen) complexed obtained potentiometrically, which was found to be 8.8. This interesting finding leads to the

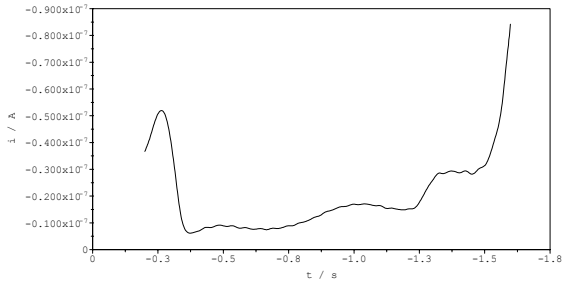

(a) (b)

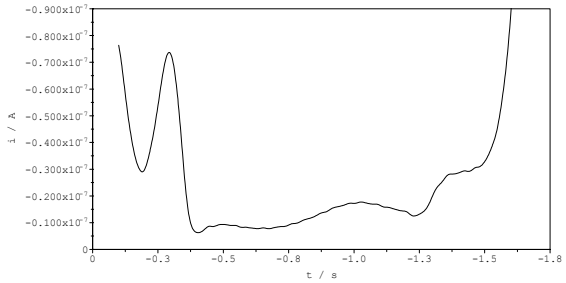

(c) (d)

(e) (f)

(g) (h)

Figure 24: Differential pulse polarograms [(a) to (h)] of cyclen-Zn(II) complex as a function of pH. The pH values for each polarogram are as follows: (a) 4.47, (b) 5.56, (c) 6.64, (d) 7.23, (e) 8.30, (f) 9.30, (g) 10.20, (h) 11.08

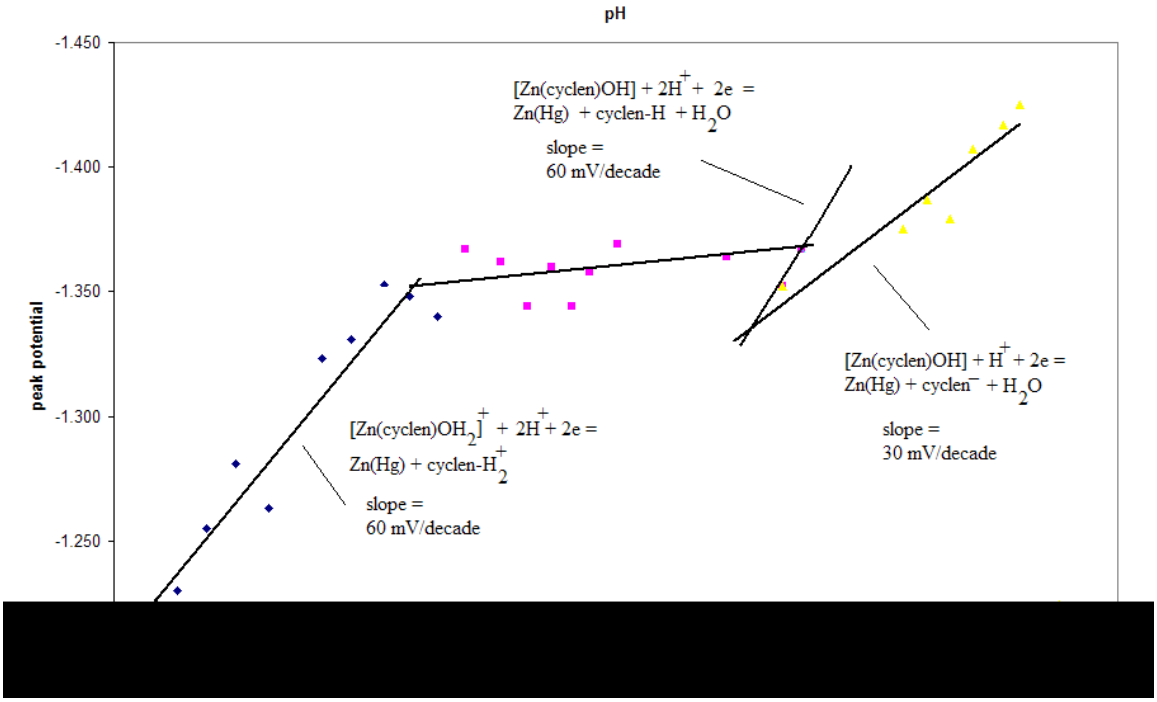

Figure 25: Plot of peak potential (E) as a function of pH for the Zn(cyclen) complex.

possible determination of pK_a values for complexes at low concentration with the use of polarography, which to our knowledge has not be utilized to a great extent. This shows the effectiveness of polarography, especially at low concentration of metal ion, for obtaining valuable information where potentiometry fails to do so.